CrystEngComm

ROYAL SOCIETY OF CHEMISTRY

COMMUNICATION

View Article Online
View Journal | View Issue

Cite this: *CrystEngComm*, 2025, **27**, 2805

Received 2nd January 2025,
Accepted 8th April 2025

DOI: 10.1039/d5ce00007f

rsc.li/crystengcomm

One-dimensional antiferromagnetic chain in the cation radical salt α-(BEDT-TTF)$_2$Hg(SeCN)$_2$Cl†

A. Henderson,[ab] A. Razpopov, [c] S. Biswas,[c] R. Valentí, [c] H. Cui,[d] R. Kato, [d] K. Wei,[b] J. van Tol, [b] T. Siegrist [*be] and J. A. Schlueter [*f]

Replacement of sulfur with selenium in the anion of the (BEDT-TTF)$_2$Hg(QCN)$_2$Cl (Q = S, Se) cation radical salts results in a dramatic change in the anion structure and the BEDT-TTF packing motif. Here we report the new α-(BEDT-TTF)$_2$Hg(SeCN)$_2$Cl salt that stabilizes charge disproportionation between two crystallographically independent BEDT-TTF molecules resulting in the formation of 1D spin chains perpendicular to the stacking axis.

Bis(ethylenedithio)tetrathiafulvalene (BEDT-TTF) cation radical salts continue to serve as important physical representations of various theoretical quantum systems. The arrangement of BEDT-TTF radical cations in these materials have dramatic effects on their physical properties. The κ-type packing motif, which is characterized by an approximately orthogonal arrangement of BEDT-TTF dimers,[1] has been of particular interest due to its arrangement of unpaired spins on a triangular lattice. For decades, the κ-(BEDT-TTF)$_2$Cu[N(CN)$_2$]X (X = Cl, Br) salts with polymeric cuprous anions have been extensively studied due in part to their proximity to a boundary between superconducting and antiferromagnetic regimes.[2,3] The Mott insulator ground state is changed from antiferromagnetic toward spin liquid as the triangular lattice becomes more isotropic.[4,5] Thus, κ-(BEDT-TTF)$_2$Cu$_2$(CN)$_3$ has been considered a prime spin liquid candidate[6,7] although a recent multi-frequency electron spin resonance study has identified the opening of a spin gap consistent with the formation of a valence bond solid ground state.[8–10]

As progress in the field is tied to the discovery of new materials, attention has turned to related BEDT-TTF salts with polymeric mercurous-based anions. Specifically, the κ-(BEDT-TTF)$_2$Hg(SCN)$_2$X (X = F, Cl, Br, I) salts have a similar κ-type packing motif.[11] It has been suggested that the emergent charge degrees of freedom in the κ-(BEDT-TTF)$_2$Hg(SCN)$_2$Br result in a quantum dipole liquid state.[12] In contrast, κ-(BEDT-TTF)$_2$Hg(SCN)$_2$Cl exhibits a sharp metal–insulator transition near 30 K, and evidence has been presented for an order–disorder type ferroelectric state driven by charge order within the BEDT-TTF dimers and stabilized by a coupling to the anions.[13] The metallic β″ polymorph of (BEDT-TTF)$_2$Hg(SCN)$_2$Cl enters a charge-ordered insulating state at 72 K.[14] While the Hg(SCN)$_2$Cl$^-$ anion is polymeric in the κ phase it is dimeric in the β″ polymorph.

A second family of BEDT-TTF salts with polymeric mercury-based anions is represented by the formula α-(BEDT-TTF)$_2$MHg(SCN)$_4$ (M = K, Rb, Tl, NH$_4$).[15] In contrast to the κ-phase, α-phase salts are characterized by canted herringbone stacks of BEDT-TTF molecules.[1] The α-(BEDT-TTF)$_2$(NH$_4$)Hg(SCN)$_4$ member of this family is an ambient pressure superconductor below 1.15 K,[16] while α-(BEDT-TTF)$_2$KHg(SCN)$_4$ exhibits superconductivity at 1 K under 3 kbar uniaxial pressure.[17] Replacement of the sulphur atom in thiocyanate with selenium leads to the selenocyanate anion, providing an opportunity for the formation of isostructural salts. For example, the α-(BEDT-TTF)$_2$TlHg(SeCN)$_4$ salt is isostructural to α-(BEDT-TTF)$_2$TlHg(SCN)$_4$.[18] The partially-substituted (BEDT-TTF)$_2$[TlHg(Se$_{0.875}$S$_{0.125}$CN)$_4$] salt has been reported with either a δ-type[19] or α-type[20] packing motif with semiconducting and metallic properties, respectively. Perhaps due to the increased difficulty of working with this anion, to

[a] *Department of Physics, Florida State University, Tallahassee, FL 32310, USA*
[b] *National High Magnetic Field Laboratory, 1800 E. Paul Dirac Drive, Tallahassee, FL 32310, USA*
[c] *Institut für Theoretische Physik, Goethe-Universität Frankfurt, Max-von-Laue-Straße 1, 60438 Frankfurt am Main, Germany*
[d] *Condensed Molecular Materials Laboratory, RIKEN, Wako-shi, Saitama 351-0198, Japan*
[e] *Department of Chemical and Biomedical Engineering, FAMU-FSU College of Engineering, Tallahassee, FL 32310, USA. E-mail: TSiegrist@fsu.edu*
[f] *Division of Materials Research, National Science Foundation, Alexandria, VA 22314, USA. E-mail: JSchluet@nsf.gov, JASchlueter@anl.gov*

† Electronic supplementary information (ESI) available: CIF for α-(BEDT-TTF)$_2$Hg(SeCN)$_2$Cl at 100 K (CCDC 2332997), thermal ellipsoid plots illustrating the atomic numbering schemes used for the BEDT-TTF molecules and the [Hg(SCN)$_2$Cl]$^-$ anion, Raman spectra, electron paramagnetic resonance data, specific heat data, theoretical methods, and DFT results. CCDC 2332997. For ESI and crystallographic data in CIF or other electronic format see DOI: **https://doi.org/10.1039/d5ce00007f**

our knowledge, these are the only BEDT-TTF salts containing selenocyanate.

Here we report the synthesis of the new α-(BEDT-TTF)$_2$-Hg(SeCN)$_2$Cl salt. Single crystals were prepared through the use of electrocrystallization.[21] The electrolyte consisted of a mixture of Hg(SeCN)$_2$ and [P(C$_6$H$_5$)$_4$]Cl in a 90/10 1,1,2-trichloroethane/ethanol solvent.‡

α-(BEDT-TTF)$_2$Hg(SeCN)$_2$Cl crystallizes in the monoclinic space group $P2_1/n$.§ As illustrated in Fig. 1, the two dimensional crystal structure is characterized by layers of BEDT-TTF radical cations separated by dimerized Hg(SeCN)$_2$-Cl$^-$ anions. These layers lie parallel to the *ab*-plane. Crystallographically, two unique BEDT-TTF molecules reside in the unit cell, which have been designated **A** and **B** for convenience. Through use of the established empirical correlation between the C–S and C=S bond lengths and electron donor charges in the BEDT-TTF salts,[23] the oxidation states for molecules **A** and **B** are determined to be 0.16 and 1.00 at 100 K. If an integral charge is assumed for the Hg(SeCN)$_2$Cl$^-$ anion, these values would indicate approximately neutral (+0.13) and charged (+0.87) BEDT-TTF molecules arranged in **ABAB**-type stacks with the molecules canted with respect to the stacking axis. Characteristic of α-type packing, molecules in alternate stacks are canted in opposite directions.[1] This results in zig-zag ribbons of equally charged molecules to be aligned along the *b*-axis, perpendicular to the (*a*-) stacking axis and well-separated from each other by chains of neutral BEDT-TTF molecules.

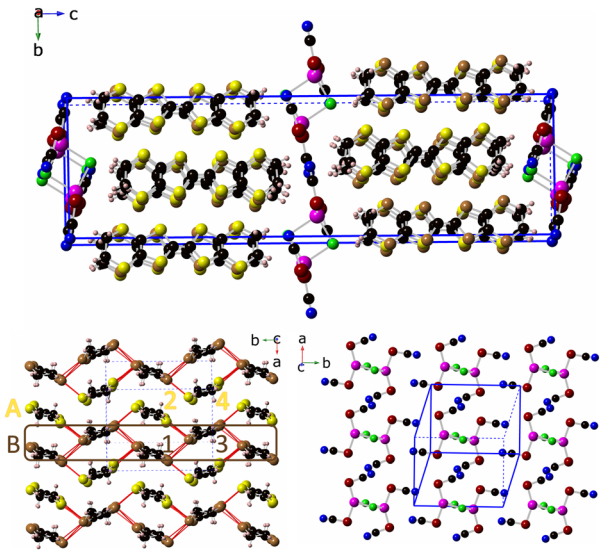

Fig. 1 (Top) Packing diagram of α-(BEDT-TTF)$_2$Hg(SeCN)$_2$Cl. (Bottom left) α-Type packing motif of the BEDT-TTF layer. The sulphur atoms in the crystallographically unique BEDT-TTF molecules are shown as yellow and brown spheres, respectively. Intermolecular S···S interactions less than 3.6 Å are indicated with red lines. The brown rectangle indicates the 1D spin chain. (Bottom right) The dimerized Hg(SCN)$_2$Cl]$^-$ anion forms a 2D structure. Colour scheme: carbon (black), sulphur (yellow/brown), hydrogen (salmon), mercury (magenta), nitrogen (blue), selenium (maroon), and chlorine (green).

Fig. 1 illustrates the α-packed layer, the charged BEDT-TTF molecules (B) are shown in brown, and the neutral (A) molecules in yellow. Each BEDT-TTF **A** molecule participates in 8 intermolecular S–S interactions shorter than 3.6 Å, the shortest of which is 3.3364(8) Å. (Fig. S3†) Within the **B** chain the shortest intermolecular S–S interaction is 3.4934(9) Å (Fig. S4†). Due to the interaction of the sulfur p-orbitals, magnetic coupling is expected. This motif is distinct from that observed at ambient temperature in the archetypical α-(BEDT-TTF)$_2$I$_3$ structure where one stack of BEDT-TTF molecules is **AAAA** type while the second is **BCBC**.[24] α-(BEDT-TTF)$_2$I$_3$ undergoes a metal-to-insulator (MI) transition at 135 K and has been proposed to be a zero-gap semiconductor under hydrostatic pressure[25] and exhibit a superconducting state under uniaxial pressure.[26] It has been shown that below the 135 K MI transition, the crystal symmetry lowers causing the **A**-stack to have **AA′AA′** packing resulting in horizontal charge ordered stripes.[27] The α′ layer of κ-α′-(BEDT-TTF)$_2$-Ag(CF$_3$)$_4$(TCE) also possesses a striped charge ordering reminiscent to that observed in α-(BEDT-TTF)$_2$Hg(SeCN)$_2$Cl.[28]

To date, no crystal structures of the Hg(SeCN)$_2$Cl$^-$ have been reported. The anion in α-(BEDT-TTF)$_2$Hg(SeCN)$_2$Cl forms a dimerized structure similar to that observed for β″-(BEDT-TTF)$_2$Hg(SCN)$_2$Cl.

Four-probe resistivity measurements were performed up to 10.5 GPa using a diamond anvil cell following the reported procedure.[29] At ambient pressure, the resistivity showed semiconducting behavior with a room-temperature value of 1500 Ω cm. The variable temperature resistivity data was not well fit by an Arrhenius plot, but the activation energy was estimated between 240 meV (room temperature) to 130 meV (240 K) (Fig. 2). The room temperature resistivity and activation energy decreased with increasing pressure, but a metallic state was not achieved over the measured pressure range.

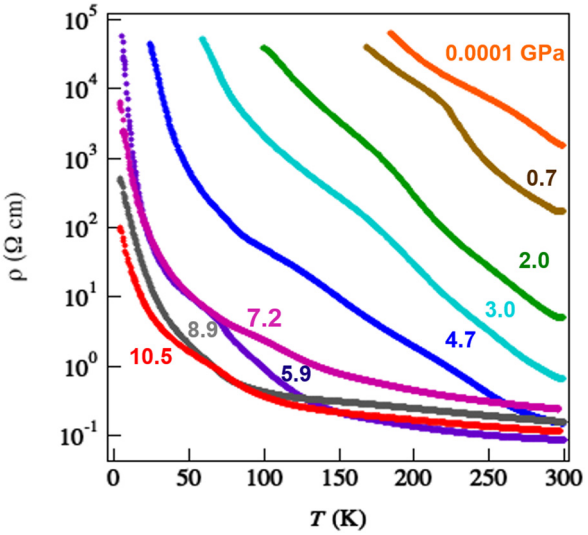

Fig. 2 Temperature dependence of electrical resistivity as a function of pressure for a single crystal of α-(BEDT-TTF)$_2$Hg(SeCN)$_2$Cl.

Because the charge order is already present at room temperature, paramagnetic behaviour is expected. Indeed, the magnetic susceptibility measurement in the temperature range between 2 K and 300 K shows paramagnetic behaviour down to a temperature of about 11.5 K, where a broad maximum of the susceptibility is observed (Fig. 3). The small feature observed at 120 K in the susceptibility with the external field perpendicular to the crystal plate is attributed to a change in the dynamics of the fluctuating terminal ethyl groups. This is also reflected in the small changes in the Raman spectra at 120 K, and in very small shifts in the EPR spectra (see ESI† material).

The broad maximum at 11.5 K is indicative of linear Heisenberg chain behaviour. In particular, the specific heat measurement does not show a peak in this temperature region (ESI† material), but a linear γ term can be extracted using a model for the specific heat of $c_p = \gamma T + \beta T^3$, with the β term modelling the lattice specific heat. Since α-(BEDT-TTF)$_2$Hg(SeCN)$_2$Cl is an insulator, the γ term is due to spin entropy. Unfortunately, integrating the linear contribution in the specific heat over an extended temperature range is hampered by the absence of a good model for the lattice specific heat. Furthermore, a Bonner–Fisher fit[30] of the magnetic susceptibility gives an interaction strength between the antiferromagnetically coupled spins of J = 18.3(1) K.

The electronic properties have been calculated using density functional theory (DFT) *via* the Perdew–Burke–Ernzerhof (PBE) functional,[31] the results are shown in Fig. 4 left panel. Two sets of bands were obtained: four bands at around −0.8 eV and four bands at the fermi level. These are the bonding and antibonding states from the BEDT-TTF molecules, respectively (see density of states in ESI† material). The antibonding states at the Fermi level predict a metallic solution which is not consistent with the observed properties in Fig. 2. It is known that DFT underestimates the correlations in these systems.[32] To resolve this issue,

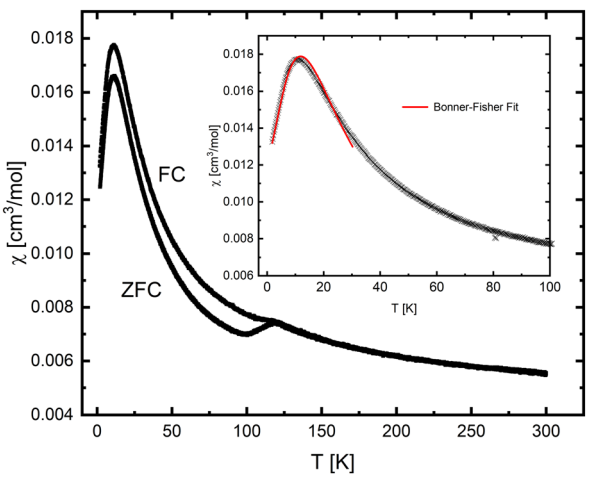

Fig. 3 Field cooled (FC) and zero-field cooled (ZFC) magnetic susceptibility data for α-(BEDT-TTF)$_2$Hg(SeCN)$_2$Cl as a function of temperature with field oriented perpendicular to the layers. Inset: A Bonner–Fisher fit to the data up to 30 K.

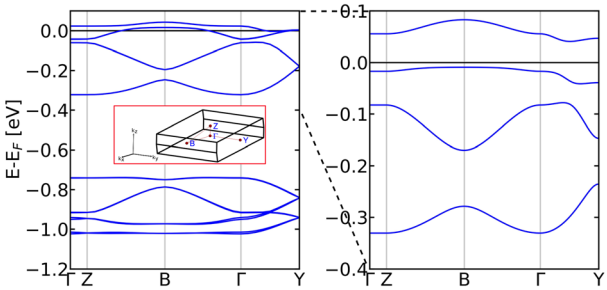

Fig. 4 Electronic band structure calculated for α-(BEDT-TTF)$_2$-Hg(SeCN)$_2$Cl along the high symmetry points Γ(0, 0, 0)–Z(0, 0, ½)–B(½, 0, 0)–Γ(0, 0, 0)–Y(0, ½, 0). The path in the Brillouin zone is displayed in the inner red panel. Left figure shows the bands obtained by DFT within the PBE functional. The right panel displays the solution obtained by the mean field approximation at filling n = 3/4 for the four band model with U = 0.25 eV. The Fermi level is set in the middle of the gap.

methods beyond DFT, namely a mean field approximation, were used. Wannier projections were performed, where each site was centered on a BEDT-TTF molecule. This results in an effective lattice of two non-interacting two dimensional sub-lattices of four sites. Because both sub-lattices of BEDT-TTF molecules are related by inversion symmetry, this leads to the same effective Hamiltonian for each BEDT-TTF layer. For this reason, only one organic BEDT-TTF layer was considered in the effective model. The model includes a lattice built with four sites connected by the dominating six nearest neighbour and strongest next nearest neighbour hoppings t_{ij} which are directly obtained *via* the Wannier parameterization and included in the kinetic part of the Hamiltonian H_{kin} (see ESI† material, Fig. S9). Using a mean-field approximation, the Hubbard Hamiltonian was solved for different parameters of the Coulomb repulsion U, where the particle number was fixed to the value obtained by the DFT calculations (filling n = ¾). A metal-to-insulator transition was found at the critical value of $U_c^{MF} \approx 0.25$ eV, with a gap opening of ≈18 meV. The mean-field solution is characterized by an antiferromagnetic type state along the sites 1 and 3 (molecules B), with magnetization, m_s = 0.69. On the other hand, the magnetization on the sites 2 and 4 (molecules A) vanishes. This agrees with the observations from the magnetic susceptibility in Fig. 3. Furthermore, the charge disproportionation between molecule A and B is also observed in the DFT results. This disproportionation is enhanced in the mean field approximation.

In summary, we have grown single crystals of a new compound in the BEDT-TTF family, α-(BEDT-TTF)$_2$-Hg(SeCN)$_2$Cl, and studied its physical properties. The charge disproportionation produces a semiconducting material that hosts a linear Heisenberg spin chain with an interaction strength of J = 18.3(1) K. The pressure dependence of the resistivity indicates that a semiconductor-to-metal transition might be reachable at higher pressures. DFT calculations confirm the semiconducting nature of the phase, with a band gap of the order of 0.18 eV.

We thank S. Hill for valuable discussions. J. A. S. acknowledges support from the Independent Research/Development program while serving at the NSF. A. R. S. B. and R. V. thank the Deutsche Forschungsgemeinschaft (DFG, German Research Foundation) for funding through TRR 288-422213477 (project A05). K. W. acknowledges support from the NHMFL. Work carried out at the NHMFL was supported by the NSF under grants DMR-1644779, DMR-2128556, and the State of Florida. A. H. and T. S. acknowledge funding from the NSF under grant DMR-1534818, DMR-1849539 and DMR-2219906. X-ray diffraction data was collected at NSF's ChemMatCARS, Sector 15 at the Advanced Photon Source (APS), Argonne National Laboratory (ANL) which is supported by the Divisions of Chemistry (CHE) and Materials Research (DMR), National Science Foundation, under grant number NSF/CHE-1834750 and NSF/CHE-2335833. This research used resources of the Advanced Photon Source, a U.S. Department of Energy (DOE) Office of Science user facility operated for the DOE Office of Science by Argonne National Laboratory under Contract No. DE-AC02-06CH11357.

Data availability

Additional data supporting this article have been included as part of the ESI.† CCDC 2332997 contains the supplementary crystallographic data for this paper.

Author contributions

T. S. and J. S. formulated the project. A. H. synthesized and crystallized the compounds. A. H., J. S., and T. S. performed the crystal structure analysis. A. R., S. B., and R. V. performed the calculations. H. C. and R. K. performed the resistivity measurements. K. W. and A. H. performed the magnetic susceptibility and specific heat measurements. J. vT. and A. H. performed the electron paramagnetic resonance measurements. A. H., T. S., and J. S. wrote the paper and all the authors contributed to revising it.

Conflicts of interest

There are no conflicts to declare.

Notes and references

‡ $Hg(SeCN)_2$ was prepared through the literature procedure,[22] while other reagents were used as received from the vendor. Single crystals of α-$(BEDT\text{-}TTF)_2Hg(SeCN)_2Cl$ were prepared through the use of electrocrystallization. A solution of 10% ethanol in 1,1,2-trichloroethane (TCE) was prepared. BEDT-TTF (15.6 mg, 0.02 mmol) was dissolved in 5 mL of the ethanol/TCE solution and placed in the anode chamber of an H-cell. $Hg(SeCN)_2$ (160.1 mg, 0.39 mmol) and $[P(C_6H_5)_4]Cl$ (164.6 mg, 0.439 mmol) were combined in 10 ml of the ethanol/TCE solution and divided between the two chambers of the H-cell. A constant current of 0.253 μA was applied for 15 weeks in an insulated dark box at ambient temperature. The crystals grew as thin black plates.

§ X-ray diffraction data was collected with synchrotron radiation. Crystal data for α-$(BEDT\text{-}TTF)_2Hg(SeCN)_2Cl$: $C_{22}H_{16}ClHgN_2S_{16}Se_2$, M = 1215.29, monoclinic, space group $P2_1/n$, a = 8.3995(4), b = 10.9240(5), c = 38.106(2) Å, β = 96.154(1), V = 3476.3(3) Å^3, Z = 4, T = 100(2) K, μ(0.41328 Å) = 1.677 mm^{-1}, D_{calc} = 2.322 g cm^{-3}, 144 387 reflections measured of which 17 779 independent (R_{int} = 0.0880), $R(F)$ = 0.0346 [13 711 data with $I > 2\sigma(I)$], w$R(F^2)$ = 0.0789. The structures were solved by direct methods (SHELXL-2014/4) and refined by full-matrix least-square on F^2 (SHELXL-2018/3).

1 T. Mori, H. Mori and S. Tanaka, *Bull. Chem. Soc. Jpn.*, 1999, **72**, 179–197.
2 M. Dumm, D. Faltermeier, N. Drichko, M. Dressel, C. Meziere and P. Batail, *Phys. Rev. B: Condens. Matter Mater. Phys.*, 2009, **79**, 195106.
3 M.-S. Nam, A. Ardavan, S. J. Blundell and J. A. Schlueter, *Nature*, 2007, **449**, 584–587.
4 K. Kanoda and R. Kato, *Annu. Rev. Condens. Matter Phys.*, 2011, **2**, 167–188.
5 B. J. Powell and R. H. McKenzie, *Rep. Prog. Phys.*, 2011, **74**, 056501.
6 Y. Shimizu, K. Miyagawa, K. Kanoda, M. Maesato and G. Saito, *Phys. Rev. Lett.*, 2003, **91**, 107001.
7 Y. Zhou, K. Kanoda and T. K. Ng, *Rev. Mod. Phys.*, 2017, **89**, 025003.
8 B. Miksch, A. Pustogow, M. J. Rahim, A. A. Bardin, K. Kanoda, J. A. Schlueter, R. Hubner, M. Scheffler and M. Dressel, *Science*, 2021, **372**, 276.
9 K. Riedl, R. Valentí and S. M. Winter, *Nat. Commun.*, 2019, **10**, 2561.
10 K. Riedl, E. Gati and R. Valentí, *Crystals*, 2022, **12**, 1689.
11 M. Z. Aldoshina, R. N. Lyubovskaya, S. V. Konovalikhin, O. A. Dyachenko, G. V. Shilov, M. K. Makova and R. B. Lyubovskii, *Synth. Met.*, 1993, **55–57**, 1905–1909.
12 N. Hassan, S. Cunningham, M. Mourigal, E. I. Zhilyaeva, S. A. Torunova, R. N. Lyubovskaya, J. A. Schlueter and N. Drichko, *Science*, 2018, **360**, 1101–1104.
13 E. Gati, J. K. H. Fischer, P. Lunkenheimer, D. Zielke, S. Kohler, F. Kolb, H. A. K. von Nidda, S. M. Winter, H. Schubert, J. A. Schlueter, H. O. Jeschke, R. Valenti and M. Lang, *Phys. Rev. Lett.*, 2018, **120**, 7.
14 W. Li, E. Rose, M. V. Tran, R. Hübner, A. Łapiński, R. Świetlik, S. A. Torunova, E. I. Zhilyaeva, R. N. Lyubovskaya and M. Dressel, *J. Chem. Phys.*, 2017, **147**, 064503.
15 A. I. Schegolev, V. N. Laukhin, A. G. Khomenko, M. V. Kartsovnik, R. P. Shibaiva, L. P. Rozenberg and A. E. Kovalev, *J. Phys. I*, 1992, **2**, 2123–2129.
16 H. H. Wang, K. D. Carlson, U. Geiser, W. K. Kwok, M. D. Vashon, J. E. Thompson, N. F. Larsen, G. D. McCabe, R. S. Hulscher and J. M. Williams, *Phys. C*, 1990, **166**, 57–61.
17 C. E. Campos, J. S. Brooks, P. J. M. van Bentum, J. A. A. J. Perenboom, S. J. Klepper, P. S. Sandhu, S. Valfells, Y. Tanaka, T. Kinoshita, N. Kinoshita, M. Tokumoto and H. Anzai, *Phys. Rev. B: Condens. Matter Mater. Phys.*, 1995, **52**, R7014–R7017.
18 R. P. Shibaeva, L. P. Rozenberg, N. D. Kushch and É. B. Yagubskii, *Crystallogr. Rep.*, 1994, **39**, 747–753.
19 R. P. Shibaeva, S. S. Khasanov, L. P. Rozenberg, N. D. Kushch, É. B. Yagubskii and E. Canadell, *Crystallogr. Rep.*, 1997, **42**, 778–782.
20 R. Rousseau, M. L. Doublet, E. Canadell, R. P. Shibaeva, S. S. Khasanov, L. P. Rozenberg, N. D. Kushch and É. B. Yagubskii, *J. Phys. I*, 1996, **6**, 1527–1553.

21 P. Batail, K. Boubekeur, M. Fourmigue and J.-C. P. Gabriel, *Chem. Mater.*, 1998, **10**, 3005–3015.
22 G. A. Bowmaker, A. V. Churakov, R. K. Harris, J. A. K. Howard and D. C. Apperley, *Inorg. Chem.*, 1998, **37**, 1734–1743.
23 P. Guionneau, C. J. Kepert, G. Bravic, D. Chasseau, M. R. Truter, M. Kurmoo and P. Day, *Synth. Met.*, 1997, **86**, 1973–1974.
24 K. Bender, I. Hennig, D. Schweitzer, K. Dietz, H. Endres and H. J. Keller, *Mol. Cryst. Liq. Cryst.*, 1984, **108**, 359–371.
25 N. Tajima, S. Sugawara, M. Tamura, Y. Nish and K. Kajita, *J. Phys. Soc. Jpn.*, 2006, **75**, 10.
26 N. Tajima, A. Ebina-Tajima, M. Tamura, Y. Nishio and K. Kajita, *J. Phys. Soc. Jpn.*, 2002, **71**, 1832–1835.
27 T. Kakiuchi, Y. Wakabayashi, H. Sawa, T. Takahashi and T. Nakamura, *J. Phys. Soc. Jpn.*, 2007, **76**, 113702.
28 J. A. Schlueter, L. Wiehl, H. Park, M. de Souza, M. Lang, H.-J. Koo and M.-H. Whangbo, *J. Am. Chem. Soc.*, 2010, **132**, 16308–16310.
29 H. Cui, J. S. Brooks, A. Kobayashi and H. Kobayashi, *J. Am. Chem. Soc.*, 2009, **131**, 6358–6359.
30 J. C. Bonner and M. E. Fisher, *Phys. Rev. A*, 1964, **135**, 640–658.
31 J. P. Perdew, K. Burke and M. Ernzerhof, *Phys. Rev. Lett.*, 1996, **77**, 3865–3868.
32 J. Ferber, K. Foyevtsova, H. O. Jeschke and R. Valent, *Phys. Rev. B: Condens. Matter Mater. Phys.*, 2014, **89**, 205106.